Microscopic model for transitions from Mott to spin-Peierls insulator in TiOCl

Yu-Zhong Zhang, Harald O. Jeschke, and Roser Valentí
Institut für Theoretische Physik, Goethe-Universität Frankfurt, Max-von-Laue-Straße 1, 60438 Frankfurt am Main, Germany
(Received 3 August 2008; published 6 November 2008)

On the basis of *ab initio* density-functional-theory calculations, we derive the underlying microscopic model Hamiltonian for TiOCl, a unique system that shows two consecutive phase transitions from a Mott insulator to a spin-Peierls insulator through a structurally incommensurate phase. We show with our model that the presence of magnetic frustration in TiOCl leads to a competition with the spin-Peierls distortion, which results in the unusual incommensurate phase. In addition, our calculations indicate that the spin-Peierls state is triggered by adiabatic phonons, which is essential for understanding the nature of the phase transition.

DOI: 10.1103/PhysRevB.78.205104 PACS number(s): 71.15.Mb, 75.10.Jm, 75.30.Et

I. INTRODUCTION

Mott insulators are materials which owe their insulating properties to strong electron correlations.[1] In practice, the Mott state is unstable against residual interactions[2] and in one dimension the dominant instability is the doubling of the unit cell via the coupling of spins to phonons, the so-called spin-Peierls transition.[3]

With the discovery in the early 1990s of the first inorganic spin-Peierls material, $CuGeO_3$,[4] followed by NaV_2O_5,[5] a large amount of work[6] was devoted to the understanding of the complexity of this instability when additional degrees of freedom such as next-nearest-neighbor interactions ($CuGeO_3$) or charge disproportionation (NaV_2O_5) are involved. Moreover, commensurate–to–structurally incommensurate transitions were observed in TTF-CuBDT (Ref. 7) and $CuGeO_3$ (Refs. 8 and 9) when a strong magnetic field is applied.

Recently, the anomalous behavior of TiOCl (Refs. 10–12)—the third inorganic spin-Peierls compound with the highest transition temperature and largest lattice distortion yet—has provoked a new debate. Upon cooling, TiOCl undergoes two consecutive phase transitions at $T_{c_2}=92$ K and $T_{c_1}=66$ K of second and first orders, respectively. These two temperatures separate a paramagnetic Mott insulator at high temperatures ($T>T_{c_2}$) from a nonmagnetic dimerized spin-Peierls state at low temperatures ($T<T_{c_1}$). In the intermediate region $T_{c_1}<T<T_{c_2}$, TiOCl shows structural incommensurabilities.[13–16] The observation of such a phase without the need to apply magnetic field is unprecedented, making the study of TiOCl compelling since this phase must be a result of the subtle competition between all interactions present in the material.

TiOCl is also unconventional in the size of the distortion $\eta=0.18$ Å observed between neighboring Ti atoms along b (Refs. 13 and 14) in the dimerized phase in contrast to, e.g., polyacetylene, where $\eta=0.08$ Å.[17] Moreover, the characteristic frequency of the spin-Peierls phonon $\Omega_0\simeq 27$ meV is comparable to the spin excitation gap $\Delta\simeq 21$ meV associated with the static dimerization in TiOCl for $T<T_{c_1}$.[16] This indicates that the anomalous spin-Peierls transition might be at the borderline between adiabatic (the phonons behave classically) and nonadiabatic (the quantum nature of the phonons is important for the phase transition) behaviors.[18–20] Moreover, increasing interest in applying pressure to TiOCl (Refs. 21–25) requires decent understanding of the phase transitions at ambient pressure.

Looking at the structure of TiOCl, this system consists of double layers of titanium (Ti) and oxygen (O) on the *ab* plane separated by chlorine (Cl) layers along the *c* direction[10,13,14] [see Fig. 1(a)]. The Ti atoms form chains along *b* with intrachain coupling J_b, whose projection on the *ab* plane gives a triangular pattern [Figs. 1(c) and 1(d)]. It has been suggested in the past[13–15] that possible frustrating interchain interactions (J_a within one layer and J_c between layers) could be responsible for the existence of the intermediate structurally incommensurate phase with a temperature-dependent modulation wave vector $\mathbf{q}=(q_1,0.5+q_2,0)$,[13,14,16] with $0<q_1,q_2\ll 0.5$. But the mechanism driving the system to such a phase has not been substantiated.

In this paper, we will demonstrate that the behavior of TiOCl can be described by a two-dimensional frustrated spin-Peierls model with large magnetoelastic coupling. We show that magnetic frustration[26] is responsible for the existence of a structurally incommensurate phase at $T_{c_1}<T<T_{c_2}$. Our results indicate that the spin-Peierls state is triggered by adiabatic phonons. The model parameters in our proposed model are calculated within *ab initio* density-functional theory (DFT) by the Car-Parrinello projector-augmented-wave (CP-PAW) method.[27]

The paper is organized as follows. Section II describes the model we propose and the details about how we determined the model parameters by DFT methods. In Sec. III we present our results on the model parameters and discuss the consistency between our results derived from the proposed model and the experimental observations. The possible mechanism for the structural incommensurability without external magnetic field is also discussed and the nature of the phonons is determined. Finally in Sec. IV we present our conclusions.

II. MODEL AND METHOD

The most general two-dimensional frustrated spin-Peierls model for TiOCl can be written as follows:

$$H=H_a+H_b+H_c, \tag{1}$$

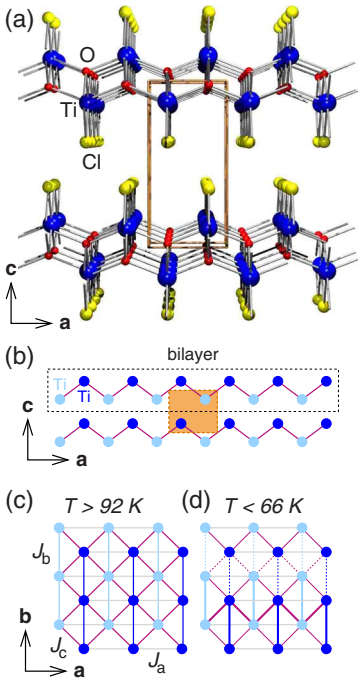

FIG. 1. (Color online) TiOCl structure and exchange interaction diagrams. (a) View along b direction of TiOCl. Here, Ti is shown as blue ball (black, largest size), O as red ball (gray, smallest size), and Cl as yellow ball (light gray, intermediate size). [(b)–(d)] Schematic views of the structure, showing only Ti ions. (b) Projection on the ac plane. Blue (black) and light blue (light gray) circles denote Ti ions in the upper and lower layers, respectively. The unit cell is shown as a shaded region. [(c) and (d)] Projections of the bilayer onto the ab plane. Ti chains run along b. Note the triangular arrangement of Ti ions. Couplings between Ti ions are shown as blue and light blue lines (black and light gray, vertical) (J_b), magenta lines (dark gray, diagonal) (J_c), and gray lines (horizontal) (J_a). The various line thicknesses signal the strengths of Ti displacements for $T<T_{c_1}$ (d) which are absent for $T>T_{c_2}$ (c).

$$H_a = J_a \sum_{i,j} \mathbf{S}_{i,j} \cdot \mathbf{S}_{i+a,j}, \tag{2}$$

$$H_b = J_b \sum_{i,j} (1 + \alpha_b d\xi_{ij,ij+b}) \mathbf{S}_{i,j} \cdot \mathbf{S}_{i,j+b} + \sum_{i,j} \frac{1}{2} K (d\xi_{ij,ij+b})^2 + \sum_{i,j} \frac{P_{b,ij}^2}{2M_b}, \tag{3}$$

$$H_c = J_c \sum_{i,j} [1 + \alpha_c d\xi_{ij,i+(a/2)j\pm(b/2)}] \mathbf{S}_{i,j} \cdot \mathbf{S}_{i+a/2,j\pm(b/2)} + \sum_{i,j} \frac{1}{2} K [d\xi_{ij,i+(a/2)j\pm(b/2)}]^2 + \sum_{i,j} \frac{P_{c,ij}^2}{2M_c}, \tag{4}$$

where $d\xi_{ij,kl}$ denote the displacements of the Ti ions on the ab plane, $d\xi_{ij,kl}=\xi_{ij,kl}-\xi^0_{ij,kl}$. Here, $\xi_{ij,kl}=|\mathbf{r}_{ij}-\mathbf{r}_{kl}|$ is the distance between two Ti ions and $\mathbf{r}_{ij}=\mathbf{r}^0_{ij}+\mathbf{u}_{ij}$ is the Ti position for $T<T_{c_1}$ [Fig. 1(d)] obtained by adding a displacement $\mathbf{u}_{ij}$ to the original Ti position $\mathbf{r}^0_{ij}$ for $T>T_{c_2}$ [Fig. 1(c)]. α_b and α_c denote the spin-phonon couplings and K is the elastic constant. M_b and M_c are the effective masses obtained by weighted summation of the masses of Ti, O, and Cl atoms and $P_{b,ij}$ and $P_{c,ij}$ denote the momentum at site (i,j) along b and c, respectively. Displacements along a are not included since they are absent in the low-symmetry structure.[13,14]

In order to obtain the model parameters from first-principles analysis, a fully relaxed $T>T_{c_2}$ crystal structure is needed. Calculations with various functionals [generalized gradient approximation (GGA) and GGA+U] with the CP-PAW method showed that the lattice parameters as well as distances and angles from GGA+U are more consistent with experimental results than those from GGA, demonstrating the importance of including electron-correlation effects for the description of the lattice properties of TiOCl,[28,29] even if it is done at the simple level of GGA+U. Moreover, our CP-PAW calculations are all carefully checked to be fully converged with respect to the size of the basis set.

The magnetic-exchange coupling constants $J_i=J_b,J_a,J_c$ were obtained from total CP-PAW energy differences between the relevant ferromagnetic (FM) and antiferromagnetic (AFM) Ti spin configurations, $E_{\mathrm{FM}}-E_{\mathrm{AFM}}$, by relating them to the J_i through mapping to the classical Heisenberg model. The determination of the spin-phonon couplings α_b and α_c was more elaborate. Out of the phonon spectrum of TiOCl for the high-symmetry ($T>T_{c_2}$) and the low-symmetry (dimerized) ($T<T_{c_1}$) phases,[28] the spin-Peierls phonon was identified and found to be degenerate in energy (A_g and B_u). The displacement vector for the Ti atoms, $\mathbf{u}_{\substack{i\\j+1}}=(0.0,\mp 0.0223,\pm 0.0403)\delta$, corresponding to the spin-Peierls phonon, was then calculated by diagonalizing the dynamical matrix, where δ is the order parameter, with $\delta=2$ corresponding to the displacements of the Ti atoms in the dimerized phase. We obtained α_c by calculating the difference in energy between the FM and a spin $S=2$ AFM spin arrangement of the unit cell doubled in both the b and c directions and distorted according to the displacement vectors $\mathbf{u}_{ij}$ for $\delta=2$. α_b was calculated analogously. We performed the calculations for various U values and found that J_c and J_a are always FM and relatively small compared to the exchange coupling J_b. The latter is always AFM and decreases monotonously as U increases, roughly fulfilling the relation $J\sim 1/U$. We have also performed linearized augmented plane-wave (LAPW) calculations with the WIEN2K (Ref. 30) code to check these results, and we obtain good agreement between both methods.

The elastic constant K was calculated by using the expression $E(\delta)=E(0)+0.0072NK\delta^2/2$, where N is the number of Ti ions in the unit cell and the numerical factor in the δ^2 term arises from the relationship between δ and $d\xi$ [see Eq. (4)]. $E(\delta)$ is the CP-PAW ground-state energy obtained for distorted lattices according to the spin-Peierls $\mathbf{u}_{ij}$ vectors given above. K was found to be almost independent of the choice of U.

III. RESULTS AND DISCUSSIONS

For the moderate value $U=1.65$ eV,[31] we obtain the model parameters $J_b=660.1$ K, $J_c=-16.7$ K, $J_a=-10.5$ K,

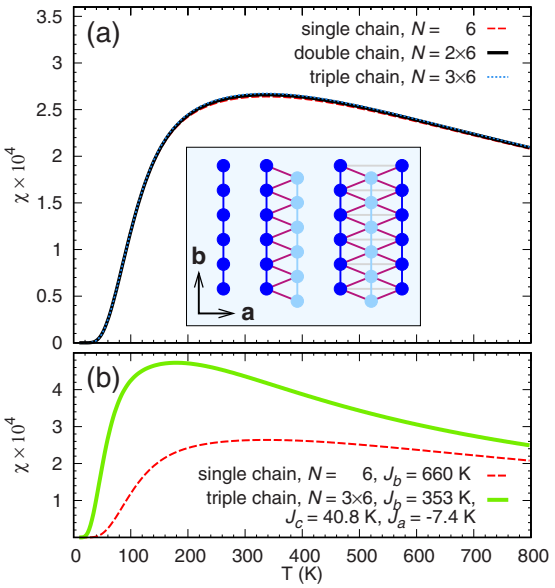

FIG. 2. (Color online) Exact-diagonalization results for spin susceptibility. (a) Susceptibility, calculated with the model parameters determined at $U=1.65$ eV. The one-, two-, and three-chain geometries are shown in the inset. Vertical, diagonal, and horizontal bonds denote the J_b, J_c, and J_a exchange couplings, respectively. Blue (black) and light blue (light gray) circles denote Ti ions in upper and lower layers, respectively, as in Fig. 1. (b) Susceptibility calculated with the model parameters of Ref. 32, which clearly disagrees with the susceptibility calculated for the experimentally determined coupling $J_b=660$ K.

$\alpha_b=1.73$ Å^{-1}, $\alpha_c=8.86$ Å^{-1}, and $K=0.292$ eV/Å^2. The reliability of these parameters is demonstrated by comparing the spin susceptibilities among single-, double-, and triple-chain Heisenberg models calculated by exact diagonalization (ED) [see Fig. 2(a)]. The behavior of the spin susceptibility at moderate to high temperatures remains almost unchanged when interchain couplings J_c and J_a are gradually introduced from single- to triple-chain models. This insensitivity of the susceptibility to the interchain couplings explains why initially TiOCl was described as a good realization of a one-dimensional spin-1/2 system[10] since the experimental data could be perfectly fitted to a one-dimensional spin-1/2 Heisenberg chain. Our results show that the experimental susceptibility is well described by a frustrated model. In contrast, a recent estimate of the magnetic interactions given by Macovez *et al.*[32] for TiOCl with $J_b=353$ K, $J_a=-7.4$ K, and $J_c=40.8$ K shows in our ED calculations considerable deviations from the experimental susceptibility as shown in Fig. 2(b).

The obtained values of J_a and J_c are the key to understanding the two consecutive phase transitions in TiOCl. The cooperation of J_a and J_c ($2J_c+J_a=-43.9$ K) in competition with J_b on a Ti site is in the range of energies where the incommensurability happens in the system (between $T_{c_1}=66$ K and $T_{c_1}=92$ K). Starting from the nonmagnetic dimerized phase, this ferromagnetic interaction together with thermal fluctuations suppresses the formation of dimer states in favor of formation of spin-1/2 solitons, leading to a structurally incommensurate phase. In Fig. 3 we present an illustration of the process. As the temperature increases, the ferromagnetic coupling breaks the central spin-zero dimer into a triplet state, and the neighboring spins get partially polarized. These spins feel the attraction (repulsion) of the central Ti $S=1/2$ spins depending on whether their interaction is favorable (unfavorable) according to J_a, J_c, and J_b. Consequently, helped by the thermal fluctuations, the neighboring Ti atoms will displace toward (away from) the central spins [see Fig. 3(b)]. This displacement will propagate to the next-nearest-neighbor atoms so that a sinusoidal atomic displacement (soliton) over many unit cells along the a and the b directions will appear, which defines the incommensurability along a and b observed experimentally.

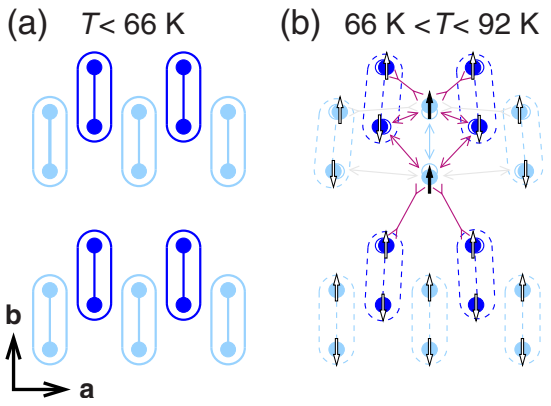

FIG. 3. (Color online) Explanation of incommensurate structure. Here, blue (black) and light blue (light gray) circles denote Ti ions in upper and lower layers, respectively, as in Fig. 1. (a) Dimerized structure at temperatures below $T_{c_1}=66$ K. The antiferromagnetic interactions and spin-phonon coupling along b lead to the formation of stable singlets. (b) Above $T_{c_1}=66$ K, thermal fluctuations lead to a competition between antiferromagnetic interactions along b and frustrating ferromagnetic interactions along a and c. We illustrate the effect on the atomic positions by showing the result of a spin flip in the central Ti dimer (black solid spins). The resulting attractive (inward arrows) or repulsive (outward arrows) interactions [gray (light gray) line, J_a, and magenta (dark gray) line, J_c] lead to modulations of the Ti atom positions along a and b directions, explaining the formation of an incommensurate structure.

The couplings in TiOCl reveal still further important features of the spin-Peierls phase transition. Since $J_b \gg J_a, J_c$, we can define a dimensionless magnetoelastic coupling constant, which uniquely determines the properties of the system, as $\lambda=J_b\alpha_b^2/K$ with $\lambda_{\mathrm{DFT}}=0.58$ as calculated from our model parameters for TiOCl. This value is significantly larger than $\lambda=0.32$ for polyacetylene.[17] With λ we can now tackle the question of whether the spin-Peierls transition is adiabatic or nonadiabatic.

We analyze H_b [Eq. (3)] in the adiabatic limit by: (i) using the mean-field (MF) approximation after applying a Jordan-Wigner transformation (see Appendix) and (ii) performing ED calculations for chains with up to 24 spins at $T=0$. In Fig. 4(a), we show the distortion of the lattice, η, as a function of the coupling constant λ for the two calculations. The MF approximation predicts a $\lambda_{\mathrm{MF}}\approx 0.56$ to induce the experimental distortion. Note that this λ_{MF} is very close to our *ab initio* determined value λ_{DFT}. ED results qualitatively

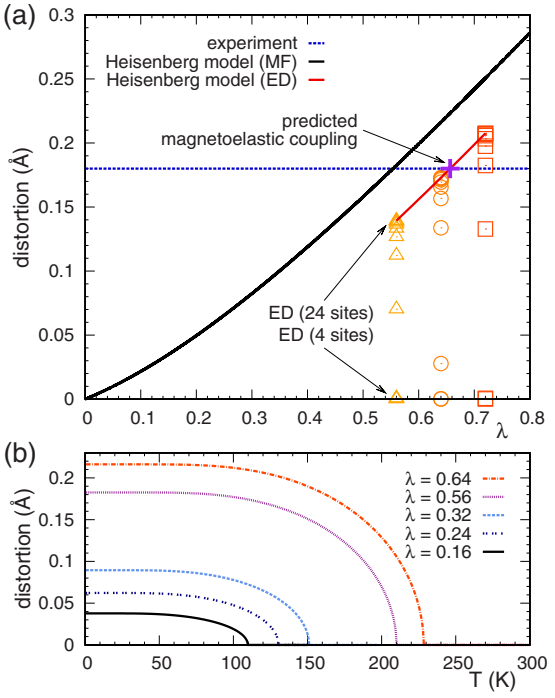

FIG. 4. (Color online) Predictive power of calculated model parameters. (a) Lattice distortion η as a function of the magnetoelastic coupling λ obtained from various approaches: Heisenberg model in mean-field approximation (black curve) and exact-diagonalization calculations for systems of up to 24 sites (symbols) for $\lambda=0.56$ (triangles), 0.64 (circles), and 0.72 (squares). Note that sizes of $N=24$ are large enough to reach converged results. The horizontal dashed line denotes the experimental η. (b) Lattice distortion η as a function of temperature for various λ obtained for H_b in the mean-field approximation. The second-order nature of the T_{c_2} phase transition is evident from the curves.

agree with the MF results and predict a $\lambda_{ED}\approx 0.64$ to describe the experimental distortion. This agreement between λ_{DFT} and λ_{MF} or λ_{ED} demonstrates the high degree of consistency in our calculations. In Fig. 4(b), we show the temperature dependence of the phase transition within the MF approach for different λ values. We observe that the spin-Peierls phase transition is of second order and the critical temperature T_{SP} lies between 100 and 230 K depending on the choice of λ, which is not far away from the experimental T_{c_2}. As is well known, inclusion of interchain couplings and strong correlation in the calculation further reduce T_{SP} to the experimental value T_{c_2}.

We now consider H_b [Eq. (3)] in the nonadiabatic limit. After quantizing the lattice degrees of freedom by introducing the phonon-creation and -annihilation operators and integrating out the phonon degrees of freedom, an effective J_1-J_2 model is obtained, where $J_2=(J_b\alpha_b)^2/4M_b\Omega_0^2\approx 0.036J_b$ and $J_1=J_b+2J_2\approx 1.07J_b$ ($\Omega_0=2\sqrt{K/M_b}$ is the bare phonon frequency). Since the ratio $J_2/J_1<0.24$,[33] nonadiabaticity will not affect the dimerization in TiOCl [in contrast to the situation in $CuGeO_3$ (Refs. 19 and 20)]. In fact, with our calculated model parameters, we find that $\Omega_0/T_{SP}\approx 2$ fulfills the condition $\Omega_0/T_{SP}<2.2$ (Ref. 20) for the occurrence of a soft phonon. Out of these two limiting calculations, we conclude that the main features of TiOCl can be well described in the adiabatic limit, in agreement with recent experiments.[16]

IV. CONCLUSIONS

The presented work shows that TiOCl is described by a frustrated spin-Peierls model on an anisotropic triangular lattice with intrachain AFM and interchain FM interactions and large magnetoelastic coupling. This is in contrast with previous suggestions on the magnetic interactions. With this model we can account for the Mott to spin-Peierls insulator phase transition in TiOCl and for the existence of intermediate zero-field structural incommensurabilities. This work also shows that the combination of *ab initio* DFT calculations with effective models is a powerful tool for describing the microscopics of this Mott insulator.

ACKNOWLEDGMENTS

We acknowledge useful discussions with L. Pisani, C. Gros, F. Essler, M. Mostovoy, D. Khomskii, C. Walther, P. Blöchl, M. Sing, and R. Claessen. We thank the Deutsche Forschungsgemeinschaft for financial support through the TRR/SFB 49 and Emmy Noether programs, and we gratefully acknowledge support by the Frankfurt Center for Scientific Computing.

APPENDIX: MEAN-FIELD-MODEL CALCULATIONS

By means of a Jordan-Wigner transformation, a spinless fermion model is obtained from H_b [Eq. (3)],

$$\frac{H_b'}{J_b}=\sum_i[1+(-1)^i\Delta]\left[\frac{1}{2}(c_i^\dagger c_{i+1}+\text{H.c.})+\left(n_i-\frac{1}{2}\right)\times\left(n_{i+1}-\frac{1}{2}\right)\right]+\sum_i\frac{1}{2}\frac{\Delta^2}{\lambda},\tag{A1}$$

where $\Delta=\alpha_b\xi_{ij,ij+b}$, $c_i^\dagger(c_i)$ is the creation (annihilation) operator of an electron, and $n_i=c_i^\dagger c_i$. Applying the Hartree-Fock approximation to the interaction part and with the help of Fourier transformation and unitary transformation, three coupled self-consistent equations can be obtained from $\frac{\partial F}{\partial\Delta}|_\mu=0$, $\frac{\partial F}{\partial b_0}|_\mu=0$, and $\frac{\partial F}{\partial\delta b}|_\mu=0$, where F is the free energy and the chemical potential μ is adjusted to yield the correct filling, i.e., $N_e=\frac{1}{\beta}\frac{\partial}{\partial\mu}\ln\Xi$. Here, $\beta=1/k_BT$ and Ξ is the grand canonical partition function,

$$\ln\Xi=\sum_{k,\pm}\ln[1+e^{-\beta[\epsilon_{HF}^{\pm}(k)-\mu]}],\tag{A2}$$

where the band structure $\epsilon_{HF}^{\pm}(k)=\pm\sqrt{E(k)}$ and

$$E(k)=(1-\Delta)^2\left(\frac{1}{2}-b_0+\delta b\right)^2+(1+\Delta)^2\left(\frac{1}{2}-b_0-\delta b\right)^2+(1-\Delta^2)\left[\left(\frac{1}{2}-b_0\right)^2-(\delta b)^2\right]2\cos k.\tag{A3}$$

b_0 and δb are defined as $(\langle c_i^\dagger c_{i+1}\rangle+\langle c_{i+1}^\dagger c_{i+2}\rangle)/2$ and

$(\langle c_i^\dagger c_{i+1}\rangle - \langle c_{i+1}^\dagger c_{i+2}\rangle)/2$, respectively. Finally, the self-consistent equations read

$$\Delta = \frac{\lambda}{2}\left[\frac{1}{N_e}\sum_k \{f[\epsilon_{\mathrm{HF}}^-(k)] - f[\epsilon_{\mathrm{HF}}^+(k)]\}\frac{1}{2\sqrt{E(k)}}\frac{\partial E(k)}{\partial \Delta} - 4b_0\delta b\right], \tag{A4}$$

$$b_0 = \frac{1}{4}\left[\frac{1}{N_e}\sum_k \{f[\epsilon_{\mathrm{HF}}^-(k)] - f[\epsilon_{\mathrm{HF}}^+(k)]\}\frac{1}{2\sqrt{E(k)}}\frac{\partial E(k)}{\partial b_0} - 4\Delta\,\delta b\right], \tag{A5}$$

$$\delta b = \frac{1}{4}\left[\frac{1}{N_e}\sum_k \{f[\epsilon_{\mathrm{HF}}^-(k)] - f[\epsilon_{\mathrm{HF}}^+(k)]\}\frac{1}{2\sqrt{E(k)}}\frac{\partial E(k)}{\partial\, \delta b} - 4\Delta b_0\right], \tag{A6}$$

where $f(\epsilon)$ is the Fermi distribution function.

[1] N. F. Mott, *Metal-Insulator Transitions* (Taylor & Francis, London, 1990).
[2] M. Imada, A. Fujimori, and Y. Tokura, Rev. Mod. Phys. **70**, 1039 (1998).
[3] *Extended Linear Chain Compounds*, edited by J. S. Miller (Plenum, New York, 1983), Vol. 3.
[4] M. Hase, I. Terasaki, and K. Uchinokura, Phys. Rev. Lett. **70**, 3651 (1993).
[5] M. Isobe and Y. Ueda, J. Phys. Soc. Jpn. **65**, 1178 (1996).
[6] P. Lemmens, G. Güntherodt, and C. Gros, Phys. Rep. **375**, 1 (2003).
[7] V. Kiryukhin, B. Keimer, and D. E. Moncton, Phys. Rev. Lett. **74**, 1669 (1995).
[8] V. Kiryukhin, B. Keimer, J. P. Hill, and A. Vigliante, Phys. Rev. Lett. **76**, 4608 (1996).
[9] T. Lorenz, B. Büchner, P. H. M. van Loosdrecht, F. Schönfeld, G. Chouteau, A. Revcolevschi, and G. Dhalenne, Phys. Rev. Lett. **81**, 148 (1998).
[10] A. Seidel, C. A. Marianetti, F. C. Chou, G. Ceder, and P. A. Lee, Phys. Rev. B **67**, 020405(R) (2003).
[11] M. Hoinkis, M. Sing, J. Schäfer, M. Klemm, S. Horn, H. Benthien, E. Jeckelmann, T. Saha-Dasgupta, L. Pisani, R. Valentí, and R. Claessen, Phys. Rev. B **72**, 125127 (2005).
[12] P. Lemmens, K. Y. Choi, R. Valentí, T. Saha-Dasgupta, E. Abel, Y. S. Lee, and F. C. Chou, New J. Phys. **7**, 74 (2005).
[13] M. Shaz, S. van Smaalen, L. Palatinus, M. Hoinkis, M. Klemm, S. Horn, and R. Claessen, Phys. Rev. B **71**, 100405(R) (2005).
[14] A. Krimmel, J. Strempfer, B. Bohnenbuck, B. Keimer, M. Hoinkis, M. Klemm, S. Horn, A. Loidl, M. Sing, R. Claessen, and M. v. Zimmermann, Phys. Rev. B **73**, 172413 (2006).
[15] R. Rückamp, J. Baier, M. Kriener, M. W. Haverkort, T. Lorenz, G. S. Uhrig, L. Jongen, A. Möller, G. Meyer, and M. Grüninger, Phys. Rev. Lett. **95**, 097203 (2005).
[16] E. T. Abel, K. Matan, F. C. Chou, E. D. Isaacs, D. E. Moncton, H. Sinn, A. Alatas, and Y. S. Lee, Phys. Rev. B **76**, 214304 (2007).
[17] C. S. Yannoni and T. C. Clarke, Phys. Rev. Lett. **51**, 1191 (1983).
[18] R. J. Bursill, R. H. McKenzie, and C. J. Hamer, Phys. Rev. Lett. **83**, 408 (1999).
[19] G. S. Uhrig, Phys. Rev. B **57**, R14004 (1998).
[20] C. Gros and R. Werner, Phys. Rev. B **58**, R14677 (1998).
[21] C. A. Kuntscher, S. Frank, A. Pashkin, M. Hoinkis, M. Klemm, M. Sing, S. Horn, and R. Claessen, Phys. Rev. B **74**, 184402 (2006).
[22] M. K. Forthaus, T. Taetz, Angela Möller, and M. M. Abd-Elmeguid, Phys. Rev. B **77**, 165121 (2008).
[23] S. Blanco-Canosa, F. Rivadulla, A. Pineiro, V. Pardo, D. Baldomir, D. I. Khomskii, M. M. Abd-Elmeguid, M. A. Lopez-Quintela, and J. Rivas, arXiv:0806.0230 (unpublished).
[24] C. A. Kuntscher, A. Pashkin, H. Hoffmann, S. Frank, M. Klemm, S. Horn, A. Schönleber, S. van Smaalen, M. Hanfland, S. Glawion, M. Sing, and R. Claessen, Phys. Rev. B **78**, 035106 (2008).
[25] Y.-Z. Zhang, H. O. Jeschke, and R. Valentí, Phys. Rev. Lett. **101**, 136406 (2008).
[26] A. P. Ramirez, Nature (London) **421**, 483 (2003).
[27] P. E. Blöchl, Phys. Rev. B **50**, 17953 (1994).
[28] L. Pisani, R. Valentí, B. Montanari, and N. M. Harrison, Phys. Rev. B **76**, 235126 (2007).
[29] L. Pisani and R. Valentí, Phys. Rev. B **71**, 180409(R) (2005).
[30] P. Blaha, K. Schwarz, G. Madsen, D. Kvaniscka, and J. Luitz, in *WIEN2K, An Augmented Plane Wave+Local Orbitals Program for Calculating Crystal*, edited by K. Schwarz (Vienna University of Technology, 2001).
[31] By comparing the density of states (DOS) and the gap, we note that the U values used in the CP-PAW ($U=1.65$ eV in our case) correspond to larger U values in WIEN2K ($U=3.3$ eV) due to the different implementations of GGA+U in these two approaches. For instance, we obtained within LAPW for $U=3.3$ eV the following: $J_b=613.4$ K, $J_c=-16.1$ K, and $J_a=-7.3$ K, which compare very well with the CP-PAW results for $U=1.65$ eV.
[32] R. Macovez, J. Luzon, J. Schiessling, A. Sadoc, L. Kjeldgaard, S. van Smaalen, D. Fausti, P. H. M. van Loosdrecht, R. Broer, and P. Rudolf, Phys. Rev. B **76**, 205111 (2007).
[33] S. Eggert, Phys. Rev. B **54**, R9612 (1996).